Controllable optical bistability of an asymmetric cavity containing a single two-level atom

Xiuwen Xia,[1,2] Jingping Xu,[1,*] and Yaping Yang[1]

[1]*MOE Key Laboratory of Advanced Micro-Structure Materials, School of Physics Science and Engineering, Tongji University, Shanghai 200092, People's Republic of China*

[2]*School of Mathematics and Physics, Jinggangshan University, Ji'an, Jiangxi 343009, People's Republic of China*

(Received 6 May 2014; revised manuscript received 31 July 2014; published 28 October 2014)

Optical bistability of a single-mode cavity containing a two-level atom in the Purcell regime has been analyzed. Compared with the case of a symmetric cavity, we find that the bistable regime of input power in an asymmetric cavity can be controlled by adjusting the cavity-loss rates of the asymmetric walls. Such results provide an optimal window of input power to realize giant optical nonreciprocity, which has promising application as the smallest all-optical diode unit with low operation power and high transmitted contrast.

DOI: 10.1103/PhysRevA.90.043857 PACS number(s): 42.65.Pc, 42.50.Pq, 42.50.Ct, 42.50.Gy

I. INTRODUCTION

A cavity containing a two-level atom or quantum dot is a classical model in quantum optics. There were many works concerning such a simple model in the last century. However, with the development of atomic manipulation and nanotechnology, it still has attracted much attention in recent years due to its significant nonlinear character. In 1995 an experiment of detuned light transmitting through an atom-cavity system showed considerable optical nonlinearity [1], and then a giant optical nonlinearity was discovered in both strong [2–4] and weak resonant coupling regimes [5,6]. By far, many applications to quantum optical devices based on giant optical nonlinearity have been proposed, such as quantum phase gates [4,7], a cavity with controllable reflectivity [8], a pulse-shape shaping scheme [9,10], a quantum states transmission scheme [11], photon nonlocal entanglement [12], an ultrafast all-optical switch [13,14], a quantum memory and all-optical transistor [14,15], a single photon nondestructive detector [16], and so on.

However, there was little work focusing on single-atom optical bistability in asymmetric cavities. Since optical bistability was proposed and realized first in Fabry-Perot resonators [17], most works have focused on understanding bistability within loss [18–22] or gain mediums [23,24] in symmetric systems, and only a few works discussed single-atom bistability [25] or bistability in asymmetric systems [26]. Various forms of bistability, known as counterclockwise, clockwise, and butterfly bistability, have been observed in the reflection in the laser amplifier cavity, while the transmission has only counterclockwise bistability [23,26].

Different from previous models, we focus on the transmission bistability of an asymmetric cavity containing a single two-level emitter. To get the single-atom optical bistability, the cavity is further limited to the Purcell regime, where the atom-cavity coupling is stronger than the atomic decay rate but smaller than the cavity-loss rates [6,27]. In this work, we find the conditions to achieve single-atom optical bistability in both a symmetric and asymmetric cavity. More interesting, it shows that the bistable regime of input power can be controlled by adjusting the asymmetric boundaries of the cavity, which provides a promising application as a single-atom all-optical switch and diode.

This paper is organized as follows. In Sec. II, we establish the coupled-mode equations concerning the asymmetric cavity containing a two-level atom. In Sec. III, single-atom optical bistability is analyzed theoretically. Its application as an optical diode with high transmitted contrast is discussed. Finally, we draw the conclusion in Sec. IV.

II. THEORETICAL MODEL

We consider a two-level atom with transition frequency ω_a embedded in the center of a single-mode cavity with frequency ω_c, as shown in Fig. 1. Different from the previous works concerning symmetric cavities [6] or a single side cavity [7], the cavity considered here can be asymmetric, whose cavity-loss rates k_1 and k_2 of the walls are different from each other in general. If the external input field ($b_{\rm in}$) is incident on left wall (M_1) of the cavity and transmits through the right wall (M_2), we define it as the forward input case, as shown in Fig. 1. Meanwhile the backward input case is the opposite one, in which input field is incident from M_2 to M_1.

In a frame rotating with the frequency of input field ω_L, the Hamiltonian concerning the atom and the cavity mode is

$$H_{\rm ac} = \hbar\Delta S_z + \hbar(\Delta+\delta)a^\dagger a + \hbar\Omega(S_+ a + a^\dagger S_-), \quad (1)$$

where a is the annihilation operator of the cavity mode. $S_- = |g\rangle\langle e|$ and $S_z = (|e\rangle\langle e| + |g\rangle\langle g|)/2$ are atomic pseudospin operators. $\Delta = \omega_a - \omega_L$ is the detuning between the atom and input field, and $\delta = \omega_c - \omega_a$ the detuning between the cavity mode and the atom. Ω is the atom-cavity coupling strength.

In order to discuss the input-output problem, operators of input field $b_{\rm in}$, reflected field b_r, and transmitted field b_t should be introduced [28,29]. The input-output channels include not only cavity-mode decay into port 1 with rate k_1 and port 2 with k_2, but also atomic spontaneous decay with rate $\gamma_{\rm at}$ and cavity mode dissipation with rate $\gamma_{\rm cav}$ [7]. The expectation values of several operators are defined as $s = \langle S_-\rangle$, $s_z = \langle S_z\rangle$, $a = \langle a\rangle$, $b_{\rm in} = \langle b_{\rm in}\rangle$, $b_t = \langle b_t\rangle$. Therefore, after tendentious deduction (more details shown in Appendix), the Heisenberg-Langevin equations of the expectation values

*Corresponding author: xx_jj_pp@hotmail.com

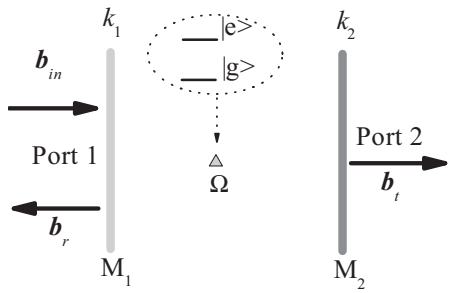

FIG. 1. Scheme of the atom-cavity coupling system under external input. Here, the cavity-loss rate k_1 (k_2) represents the decay of cavity mode into port 1 (2) through M_1 (M_2).

in the forward input case are as follows:

$$\dot{s} = -(i\Delta + \gamma_{\rm at}/2)s + 2i\Omega s_z a, \tag{2a}$$

$$\dot{s}_z = -i\Omega s^* a + i\Omega a^* s - \gamma_{\rm at}(s_z + 1/2), \tag{2b}$$

$$\dot{a} = -i(\Delta + \delta)a - (k + \gamma_{\rm cav}/2)a - i\Omega s - i\sqrt{k_1}b_{\rm in}, \tag{2c}$$

$$b_t = -i\sqrt{k_2}a. \tag{2d}$$

Here the superscript star states the complex conjugate. We only consider the expectation of operators because they can be measured by homodyne detection. With the semiclassical hypothesis the quantum correlations between atomic operators and field operators have been neglected.

In Eqs. (2) the input field is represented by $b_{\rm in}$. $k = (k_1 + k_2)/2$ is the average of two cavity-loss rates k_1 and k_2. The cavity is symmetric when $k_1 = k_2$, while it is asymmetric when $k_1 \neq k_2$. In the Purcell regime, k is much larger than $\gamma_{\rm at}$, $\gamma_{\rm cav}$, and Ω, and they fulfill the rule of $(\gamma_{\rm at}, \gamma_{\rm cav}) < \Omega < k$. Because $\gamma_{\rm cav}$ is only combined with k in Eq. (2c) and $k \gg (\gamma_{\rm cav}, \gamma_{\rm cav})$, it can be ignored. So we set $\gamma_{\rm cav} = 0$ in the following discussion without loss of generality.

In our scheme, there are breakings of time-reversal and spatial symmetries due to the dissipations and the difference between k_1 and k_2. Optical nonlinearity is inherent due to the saturation of the atom. The cavity can provide the feedback field. Thus our scheme is feasible to realize optical bistability. To discuss the optical bistability quantitatively, all the couplings and damping rates in Eqs. (2), i.e., $k_1, k_2, k, \gamma_{\rm cav}, \Omega, \Delta$, and δ, are normalized by taking $\gamma_{\rm at} \equiv 1$ in the following.

III. OPTIAL BISTABILITY AND TRANSMISSION NONRECIPROCITY

A. Optical bistability in an asymmetric cavity

Optical bistability requires two stable output states under certain input power. To get the input-output relation of our scheme, we define $n_{\rm in} = \langle b_{\rm in}^\dagger b_{\rm in}\rangle$ and $n_t = \langle b_t^\dagger b_t\rangle$ as the average incident and transmitted photon numbers per unit time, respectively. As abbreviations, we denote $n_{\rm in}$ and n_t as the input power and output power, respectively. Meanwhile, $n_c = \langle a^\dagger a\rangle$ is photon numbers per unit time in the cavity. Therefore our object is to find the relation between $n_{\rm in}$ and n_t. The procedures are as follows. As optical bistability is a steady state, the left time derivatives in Eqs. (2) all equal zeros. The relation between n_t and n_c can be first obtained through Eq. (2d) as

$$n_t = k_2 n_c. \tag{3}$$

Equation (3) indicates that n_t is proportional to n_c with factor k_2, and then from Eq. (2a) the steady atomic dipole moment s can be expressed as

$$s = \frac{2i\Omega s_z a}{i\Delta + \gamma_{\rm at}/2}. \tag{4}$$

Inserting Eqs. (3) and (4) into Eq. (2b), we obtain the steady atomic population s_z as

$$s_z = -\frac{1}{2}\frac{1}{1+y}, \tag{5}$$

where y is the saturation parameter with the expression as

$$y = n_t/P_{\rm ct}. \tag{6}$$

Here $P_{\rm ct}$ is the critical power of n_t to reach $s_z = -1/4$, satisfying

$$P_{\rm ct} = \frac{k_2\left(\Delta^2 + \gamma_{\rm at}^2/4\right)}{8\Omega^2}. \tag{7}$$

Inserting Eqs. (4) and (5) into Eq. (2c), we can relate the cavity field a to the input field $b_{\rm in}$ as

$$\left[k + \frac{\gamma_{\rm cav}}{2} + \frac{\Omega^2}{(i\Delta + \gamma_{\rm at}/2)(1+y)} + i(\Delta + \delta)\right]a = -i\sqrt{k_1}b_{\rm in}.$$

After modulus squaring both sides and combining it with Eq. (3), we finally get the relation between $n_{\rm in}$ and n_t as

$$n_{\rm in} = \frac{n_t}{k_1 k_2}\left\{\left[k + \frac{\gamma_{\rm cav}}{2} + \frac{\Omega^2\gamma_{\rm at}/2}{\left(\Delta^2 + \gamma_{\rm at}^2/4\right)(1+y)}\right]^2 + \left[(\Delta + \delta) - \frac{\Omega^2\Delta}{\left(\Delta^2 + \gamma_{\rm at}^2/4\right)(1+y)}\right]\right\}^2. \tag{8}$$

Equation (8) is the starting point of the analysis of optical bistability and nonreciprocity. Notice Eq. (8) is satisfied only for the forward input case, and this subsection is limited to the forward input case, as shown in Fig. 1.

In principle, nonlinear optical systems combined with a feedback environment may possess more than one output state for a given input state. One consequence is the optical bistability. Therefore it is possible to obtain single-atom optical bistability in the present scheme. In the following we set $\gamma_{\rm at} = 1$, $\Delta = \delta = \gamma_{\rm cav} = 0$, $\Omega = 50$, and $k = 500$ as common parameters to calculate the input-output relation. Notice that these parameters guarantee the Purcell regime's requirement, i.e., $\gamma_{\rm at} < \Omega < k$. In addition, since $k = (k_1 + k_2)/2$, we choose $k_1 = k_2 = 500$ as the symmetric cavity, and choose $k_1 = 400$ & $k_2 = 600$ and $k_1 = 600$ & $k_2 = 400$ as two kinds of asymmetric cavities. The relations of n_t and $n_{\rm in}$ are plotted in Fig. 2 to illustrate the optical bistability.

In Fig. 2(a), it shows clearly that the transmission undergoes a counterclockwise hysteresis in the symmetric cavity. There are two critical input powers n_l and n_u to identify the boundaries of the bistable regime. Thus we can distinguish the bistable regime from the so-called linear

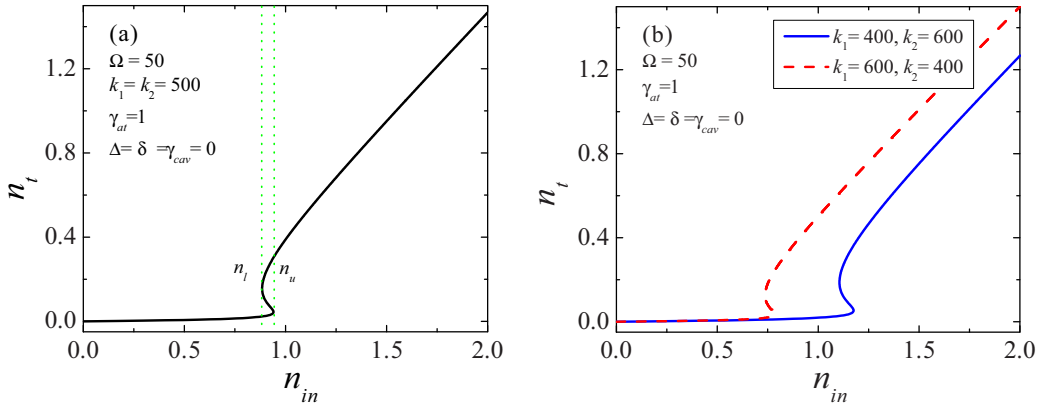

FIG. 2. (Color online) Single-atom optical bistability in the forward input case. (a) n_t vs $n_{\rm in}$ in a symmetric cavity with $k_1 = k_2 = 500$. Two vertical green dotted lines refer to the threshold intensities of bistable states n_l and n_u. (b) n_t vs $n_{\rm in}$ in two kinds of asymmetric cavities with $k_1 \neq k_2$. Common parameters are $\gamma_{\rm at} = 1$, $\Delta = \delta = \gamma_{\rm cav} = 0$, $\Omega = 50$, and $k = 500$.

regime $n_{\rm in} < n_l$, in which light is almost blocked, and from the saturation regime $n_{\rm in} > n_u$, in which light is almost transmitted.

Then we discuss the case of an asymmetric cavity. In Fig. 2(b), the solid curve refers to n_t vs $n_{\rm in}$ in the asymmetric cavity, with $k_1 = 400$ and $k_2 = 600$, while the dashed curve refers to that with $k_1 = 600$ and $k_2 = 400$. It can be seen that the threshold intensities n_l and n_u are changed due to the cavity's asymmetry. Compared with the case of a symmetric cavity in Fig. 2(a), the optical bistable regime in the asymmetric cavity with $k_1 = 400$ and $k_2 = 600$ is shifted to a higher input power, while the regime in the asymmetric cavity with $k_1 = 600$ and $k_2 = 400$ is shifted to lower input power. Figure 2(b) indicates that optical bistability can be manipulated by the asymmetry of the cavity. As we know, the cavity-loss rate k_j ($j = 1,2$) relates to the transmittivity T_j ($j = 1, 2$) of the mirror M_j ($j = 1, 2$) and the larger T_j maps the larger k_j. Therefore the bistable regime shall be lower-shifted in cavity with $T_1 > T_2$ and be higher-shifted in cavity with $T_1 < T_2$ in the forward input case.

In order to explain the above result, after inserting Eqs. (6) and (7) into Eq. (8), we can rewrite Eq. (8) as a cubic equation of output power n_t under a given input power $n_{\rm in}$, which is

$$a_0 n_t^3 + b_0(n_{\rm in}) n_t^2 + c_0(n_{\rm in}) n_t + d_0(n_{\rm in}) = 0, \tag{9}$$

where

$$\begin{aligned}
a_0 &= [(k+\gamma_{\rm cav}/2)^2 + (\Delta+\delta)^2]\left(\Delta^2+\gamma_{\rm at}^2/4\right)^2/P_{\rm ct}^2,\\
b_0(n_{\rm in}) &= 2\left[(k+\gamma_{\rm cav}/2)\left(\Delta^2+\gamma_{\rm at}^2/4\right)+\Omega^2\gamma_{\rm at}/2\right](k+\gamma_{\rm cav}/2)\left(\Delta^2+\gamma_{\rm at}^2/4\right)/P_{\rm ct}\\
&\quad + 2\left[(\Delta+\delta)\left(\Delta^2+\gamma_{\rm at}^2/4\right)-\Omega^2\Delta\right](\Delta+\delta)\left(\Delta^2+\gamma_{\rm at}^2/4\right)/P_{\rm ct} - k_1k_2\left(\Delta^2+\gamma_{\rm at}^2/4\right)^2 n_{\rm in}/P_{\rm ct}^2,\\
c_0(n_{\rm in}) &= \left[(k+\gamma_{\rm cav}/2)\left(\Delta^2+\gamma_{\rm at}^2/4\right)+\Omega^2\gamma_{\rm at}/2\right]^2 + \left[(\Delta+\delta)\left(\Delta^2+\gamma_{\rm at}^2/4\right)-\Omega^2\Delta\right]^2 - 2k_1k_2\left(\Delta^2+\gamma_{\rm at}^2/4\right)^2 n_{\rm in}/P_{\rm ct},\\
d_0(n_{\rm in}) &= -k_1k_2\left(\Delta^2+\gamma_{\rm at}^2/4\right)^2 n_{\rm in}.
\end{aligned}$$

It is obvious that optical bistability occurs when Eq. (9) has three different positive real roots [30]. Thus we can get the criteria to identify the optical bistable condition. The discriminant reads

$$P(n_{\rm in}) = B^2 - 4AC, \tag{10}$$

where $A = b_0^2 - 3a_0c_0$, $B = b_0c_0 - 9a_0d_0$, $C = c_0^2 - 3b_0d_0$. The optical bistable threshold intensities n_l and n_u can be obtained by solving $P(n_{\rm in}) = 0$.

Retaining the common parameters as $\gamma_{\rm at} = 1$, $\delta = \gamma_{\rm cav} = 0$, $k = 500$, and $\Omega = 50$, we plot the bistable threshold powers n_l and n_u vs detuning Δ in symmetric and asymmetric cavities in Fig. 3. As expected, compared to the bistability in the symmetric cavity (black curves, $k_1 = k_2 = 500$), the bistable regimes in the asymmetric cavity with $k_1 = 400$ and $k_2 = 600$ are shifted to stronger input power (blue curves), while the bistable regimes in the asymmetric cavity with $k_1 = 600$ and $k_2 = 400$ are shifted to weaker input power (red curves) in both resonant and off-resonant cases. Optical bistable phenomenon is remarkable in the resonant case but vanishes when $|\Delta| > 0.5$. Therefore, we will focus on the resonant case to illustrate how to manipulate the optical bistability with unequal cavity-loss rates k_1 and k_2 in the following.

Here we discuss the influence of the asymmetry of the cavity on the bistable regime. By fixing k, we can change the degree of the cavity's asymmetry by shifting k_1, while k_2 should vary correspondingly according to the equation $k_2 = 2k - k_1$. Adopting the common parameters, i.e., $\gamma_{\rm at} = 1$, $\Delta = \delta = \gamma_{\rm cav} = 0$, $\Omega = 50$, and $k = 500$, we plot threshold intensities n_u and n_l as functions of k_1 in Fig. 4. As expected, the bistable regime is shifted with k_1, in other words, the bistability can be controlled by the asymmetry of the cavity.

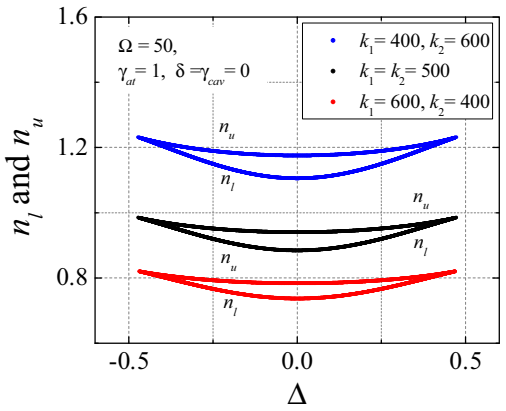

FIG. 3. (Color online) Optical bistable threshold intensities n_l and n_u vs detuning Δ in the symmetric and asymmetric cavities. $\gamma_{\rm at} = 1, \delta = \gamma_{\rm cav} = 0, \Omega = 50$, and $k = 500$.

Figure 4 also shows the way to manipulate optical bistability by adjusting the asymmetric cavity. In the forward input case, with the decrease of k_1, the optical bistable threshold intensities n_l and n_u increase and the optical bistable width $n_u - n_l$ enlarges, too. It provides us a way to shift the bistable regime to higher input power by furnishing a higher-reflective mirror in the input side and a lower-reflective mirror in the output side. By interchanging the front mirror M_1 and the back mirror M_2, we can shift the bistable regime to lower input power.

Physical insight into the controllable bistability in the asymmetric cavity is gained when one considers the different degree of atomic absorptive saturation in the two input cases. For a certain input power $n_{\rm in}$, the cavity average photon number n_c shall be larger for the case of $k_1 > k_2$ than that of $k_1 < k_2$, and the larger optical nonlinearity induced by the larger saturation shall lower the bistable threshold intensities n_l and n_u. It is the origin of the controllable bistability in the asymmetric cavity.

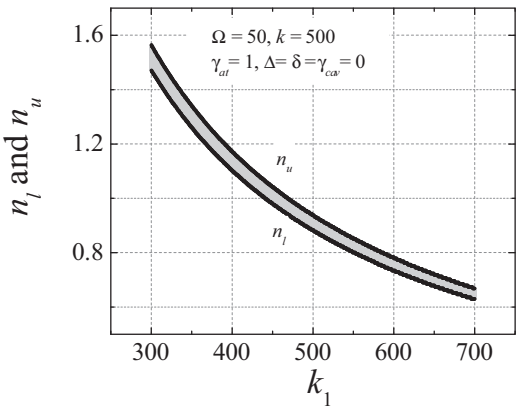

FIG. 4. Optical bistable threshold intensities n_l and n_u as functions of the left side cavity-loss rate k_1 in an asymmetric cavity. Common parameters are $\gamma_{\rm at} = 1$, $\Delta = \delta = \gamma_{\rm cav} = 0$, $\Omega = 50$, $k = 500$, and $k_2 = 2k - k_1$. Curves n_u and n_l bound the regime of optical bistability (gray area).

B. Optical nonreciprocity

Optical nonreciprocity is the essence of an optical diode. In our previous work [31], we have shown that an asymmetric nonlinear system can generate optical nonreciprocity. Due to the different degree of nonlinearity between the forward and backward input cases in the asymmetric cavity, we have introduced a considerable optical nonreciprocity in the single atom-cavity coupling system beyond optical bistability. In this work, we are aware of that a giant optical nonreciprocity can be obtained by including the controllable optical bistability in the asymmetry cavity.

As the atom is in the center of the cavity, the backward input case is equivalent to the forward input case by interchanging k_1 and k_2. It allows us to get the optical properties of the backward input case easily. For example, if we furnish the asymmetric cavity with $k_1 = 600$ and $k_2 = 400$, the input-output curve of the forward input case is the red dashed curve in Fig. 2(b), while that of the backward input case is the same with the blue solid curve in Fig. 2(b). It is clear that the behavior of the input-output of the asymmetric cavity depends on the input direction, which shows the existence of optical nonreciprocity.

In order to explore the optical nonreciprocity explicitly, we use transmittivity $T = n_t/n_{\rm in}$ to indicate the different optical character under opposite input directions. In Fig. 5, we plot the transmittivity T as a function of input power $n_{\rm in}$ for the cavity with $k_1 = 600$ and $k_2 = 400$. Other parameters are the same as those in Fig. 4. From Fig. 5(a), the solid curve refers to the case of backward input, which shows that the cavity is almost blocked until $n_{\rm in} > n_{l-b} = 1.11$ (right vertical dotted line); meanwhile, the dashed curve is the transmittivity of the forward input case, which shows that the cavity is transparent when $n_{\rm in} > n_{u-f} = 0.78$ (the left vertical dotted line). This difference originates from the influence of the cavity's asymmetry on the bistable state, as mentioned in the above section. Notice the cavity is blocked when the input power is located in the linear regime, while it is transparent when the input power is in the saturated regime.

According to Fig. 5(a), there is an optimal operation power window, i.e., $n_{\rm in} \in [n_{u-f}, n_{l-b}]$, to realize giant optical nonreciprocity. When the input power $n_{\rm in}$ falls into this window, it can transmit through the cavity for a forward incident but is blocked for a backward incident. To show this behavior clearly, we extract the transmittivity curves under such an optimal operation power window in Fig. 5(b). The curves show a typical optical diode character, which only permits light propagation in the forward input case. The transmitted contrast $C_T = 10 \times |\log_{10}(T_f/T_b)|$ is easy to reach 13 dB in the optimal operation power window. Such high contrast is due to the shift of the bistable regime induced by the asymmetric cavity.

Actually, Fig. 4 can be used to identify the optimal operator power window of nonreciprocity for the other asymmetric cavity. A larger difference between k_1 and k_2 will provide a wider optimal window. In the optimal operation power window, input power $n_{\rm in}$ is located in the linear regime for one incident direction, while it falls into the saturated regime for the opposite incident, and therefore the giant optical nonreciprocity occurs. Our predication can be used to realize

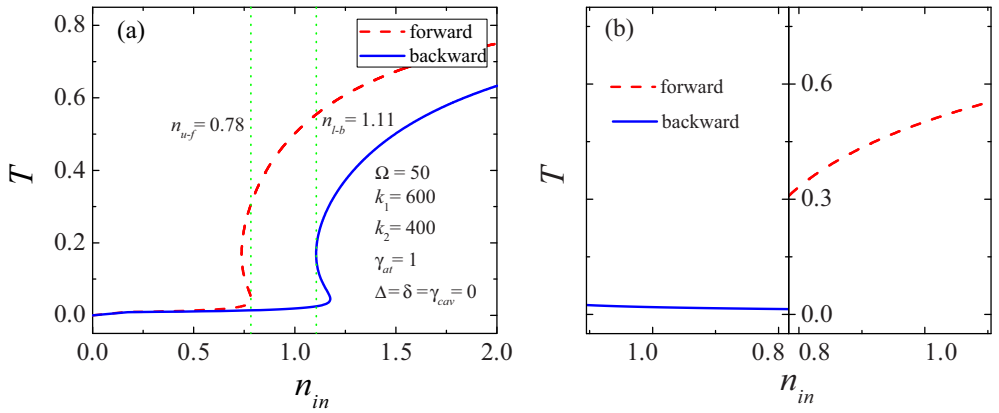

FIG. 5. (Color online) Transmittivity T as a function of input power $n_{\rm in}$ with $k_1 = 600$ and $k_2 = 400$. (a) Input power ranges from 0 to 2.0. (b) Input power falls in the optimal operation power window [0.78, 1.11]. Solid blue curves refer to the backward input case, while the dashed red curves refer to the forward input case. Common parameters are $\gamma_{\rm at} = 1$, $\Delta = \delta = \gamma_{\rm cav} = 0$, $\Omega = 50$, and $k = 500$.

single-atom optical switch, optical diodes, optical memory, and so on.

At last, we discuss the experimental possibility to observe our theoretical predictions. Recently, several atom-cavity coupling systems have been realized experimentally [7,32]. In the experiment performed in Ref. [7], a single ^{87}Rb atom is trapped by the evanescent field at about 200 nm from the surface of a single-sided photonic crystal, which is a one-sided cavity. The incident field with wavelength $\lambda = 780$ nm is resonantly coupled to the atomic transition of $|5S_{1/2}, F = 2\rangle \rightarrow |5P_{3/2}, F' = 2\rangle$. The atomic spontaneous decay rate ($\gamma_{\rm at} = 2\pi \times 6$ MHz), cavity-loss rate ($k = 2\pi \times 25$ GHz), and atom-cavity coupling strength ($\Omega = 2\pi \times 0.55$ GHz) are measured by using a polarization interferometer. This is the reason why we adopt $\gamma_{\rm at} = 1, \Omega = 50$, and $k = 500$ to perform the simulation here. To check our predication, the single-sided cavity should be extended to the asymmetric double-sided cavity and the cavity-loss rates should be lowered. The asymmetric double-sided cavity can be obtained by adding other Bragg reflectors of the cavity [33]. Or more directly, one may construct the asymmetric cavity by iron implantation and thin-film deposition based on silicon due to the development of nanotechnology. If we adopt the parameters $\gamma_{\rm at} = 2\pi \times 6$ MHz and $\lambda = 780$ nm, the operation input power $P_{\rm th}$ of optical bistability is about ten picowatts, predicted by the formula $P_{\rm th} = n_{\rm in} \times 2\pi\hbar c \times \gamma_{\rm at}/\lambda$, where c is the velocity of light in vacuum. Thus, it is feasible to realize our scheme under the present technology.

IV. CONCLUSION

We have shown that a single two-level atom in an asymmetric cavity can generate controllable optical bistability, which leads to giant optical nonreciprocity in the Purcell regime. The optical bistable conditions, as well as the controllable optical bistable effects, have been discussed in detail. According to our study, the linear, bistable, and saturated regimes can be shifted by adjusting the asymmetric walls of the cavity. Due to the controllability of optical bistable effects in the asymmetric cavity, we propose an all-optical switch, as well as a low-operation, high transmitted contrast all-optical diode based on a single atom-cavity coupling system.

ACKNOWLEDGMENTS

This work is supported in part by the National Science Foundation of China (Grants No. 11274242 and No. 11474221), the Joint Fund of the National Nature Science Foundation of China, and the China Academy of Engineering Physics (Grant No. U1330203); the National Key Basic Research Special Foundation of China (Grants No. 2011CB922203 and No. 2013CB632701); and the Fundamental Research Funds for the Central Universities.

APPENDIX: DERIVATION OF EQS. (2)

As shown in Fig. 1, the cavity mode is coupled to the outside continuum modes via two ports labeled 1 and 2 with coupling constants g_1 and g_2, respectively. The Hamiltonian of the atom-cavity coupling system under rotating-wave approximation is as follows:

$$\begin{aligned} H = {} & \hbar\omega_a S_z + \hbar\omega_c a^\dagger a + \hbar\sum_k \omega_k b_k^\dagger b_k + \hbar\sum_l \omega_l c_l^\dagger c_l \\ & + \hbar\sum_k g_1(b_k^\dagger a + a^\dagger b_k) + \hbar\sum_l g_2(c_l^\dagger a + a^\dagger c_l) \\ & + \hbar\Omega(S_+ a + a^\dagger S_-). \end{aligned} \tag{A1}$$

Here a, b_k, and c_l are the annihilation operators of the cavity mode, the modes of port 1 and port 2, respectively, while ω_c, ω_k, and ω_l are their corresponding angular frequencies. $S_- = |g\rangle\langle e|$ and $S_z = (|e\rangle\langle e| + |g\rangle\langle g|)/2$ are atomic operators. The first four terms in Eq. (A1) represent the Hamiltonian of the atom, the cavity mode, and the continuum modes in ports 1 and 2, respectively. The last three terms represent the couplings of the cavity mode, with the modes of port 1, modes of port 2, and atom, respectively. Ω is the coupling strength between the atom and cavity mode.

We follow the standard procedure. We know that Heisenberg equations of motion for an arbitrary operator fulfills

$$\frac{\partial \widehat{O}}{\partial t} = \frac{1}{i\hbar}[\widehat{O}, H]. \tag{A2}$$

From Eq. (A1), the Heisenberg equations of motion for the operators are

$$\begin{aligned}
\dot{S}_- &= -i\omega_0 S_- - i\Omega(-2S_z)a, \\
\dot{S}_z &= -i\Omega S_+ a + i\Omega a^\dagger S_-, \\
\dot{a} &= -i(\omega_0+\delta)a - i\Omega S_- - ig_1\sum_k b_k - ig_2\sum_l c_l, \\
\dot{b}_k &= -i\omega_k b_k - ig_1 a, \\
\dot{c}_l &= -i\omega_l c_l - ig_2 a.
\end{aligned} \tag{A3}$$

We find for $t > t_0$, where t_0 is a reference of time,

$$b_k(t) = b_k(t_0)e^{-i\omega_k t} - ig_1\int_{t_0}^{t} du a(u)e^{-i\omega_k(t-u)}. \tag{A4}$$

Following previous works [6,28], we define the input field operator $b_{\rm in}$ for port 1 for $t > t_0$ in the Heisenberg picture and then read

$$b_{\rm in}(t) = \frac{1}{\sqrt{\tau_k}}\sum_k b_k(t_0)e^{-i\omega_k(t-t_0)}, \tag{A5}$$

where τ is defined by

$$\sum_k e^{-i\omega_k t} = \delta(t)\tau. \tag{A6}$$

The quantity τ has the dimension of time and depends on the mode density. The quantity $b_{\rm in}^\dagger b_{\rm in}$ scales like a photon number per unit of time and represents the incoming power in port 1. Summing Eqs. (A4) over all modes and using the Markov approximation one can get

$$\sum_k b_k(t) = \sqrt{\tau_k}b_{\rm in}(t) - \frac{i}{2}g_1\tau_k a(t). \tag{A7}$$

The evolution of the operator in the Heisenberg picture holds antisymmetry of time reversal. By reversing the time and carrying out the same procedure, we can define the reflected field operator (b_r). Finally, we can get the relation between b_r and $b_{\rm in}$ and the transmitted field operator (b_t):

$$\begin{aligned}
b_r &= b_{\rm in} - i\sqrt{k_1}a, \\
b_t &= -i\sqrt{k_2}a,
\end{aligned} \tag{A8}$$

where $k_1 = g_1^2\tau_k$, $k_2 = g_2^2\tau_l$ represent the cavity-loss rates from port 1 and port 2, respectively.

After some algebra arrangement the Heisenberg equations for the slowly varying operators are finally written in the frame rotating at a fixed drive frequency ω_L:

$$\begin{aligned}
\dot{S}_- &= -i\Delta S_- - i\Omega(-2S_z)a, \\
\dot{S}_z &= -i\Omega S_+ a + i\Omega a^\dagger S_-, \\
\dot{a} &= -i(\Delta+\delta)a - ka - i\Omega S_- - i\sqrt{k_1}b_{\rm in}, \\
b_t &= -i\sqrt{k_2}a.
\end{aligned} \tag{A9}$$

Here, $\Delta = \omega_a - \omega_L$ and $\delta = \omega_c - \omega_a$ are the detunings between the bare atomic (ω_a), cavity (ω_c), and laser (ω_L) frequencies, respectively. $k = (k_1 + k_2)/2$ represents the average cavity-loss rate. These equations are the quantum coupled-mode equations for the evolution of the atom and the cavity, driven by the external fields $b_{\rm in}$. By adding the atomic and cavitary dissipations and quantum noises, the set of Eqs. (A9) should be modified as follows:

$$\begin{aligned}
\dot{S}_- &= -(i\Delta + \gamma_{\rm at}/2) + S_- - i\Omega(-2S_z)a + G, \\
\dot{S}_z &= -i\Omega S_+ a + i\Omega a^\dagger S_- - \gamma_{\rm at}(S_z + 1/2) + K, \\
\dot{a} &= -i(\Delta+\delta)a - (k + \gamma_{\rm cav}/2)a - i\Omega S_- - i\sqrt{k_1}b_{\rm in} + H, \\
b_t &= -i\sqrt{k_2}a.
\end{aligned} \tag{A10}$$

Here $\gamma_{\rm at}$ and $\gamma_{\rm cav}$ are the dissipation rates of the atom and the cavity mode, respectively, and G, K, and H are noise operators due to the interaction of the atom and the cavity with their respective reservoirs, respecting $\langle G\rangle = \langle K\rangle = \langle H\rangle = 0$. At this stage we shall restrict ourselves to the Purcell regime. With the semiclassical hypothesis the quantum correlations between atomic operators and field operators can be neglected. Therefore, we only consider the values of expectation of operators, which can be measured by homodyne detection. With the definition of dipole moment $s = \langle S_-\rangle$, atomic population $s_z = \langle S_z\rangle$, and amplitude of cavity (incident and transmitted) field $a = \langle a\rangle$ ($b_{\rm in} = \langle b_{\rm in}\rangle$ and $b_t = \langle b_t\rangle$), we obtain

$$\begin{aligned}
\dot{s} &= -i(\Delta + \gamma_{\rm at}/2)s + 2i\Omega s_z a, \\
\dot{s}_z &= -i\Omega s^* a + i\Omega a^* s - \gamma_{\rm at}(s_z + 1/2), \\
\dot{a} &= -i(\Delta+\delta)a - (k + \gamma_{\rm cav}/2)a - i\Omega s - i\sqrt{k_1}b_{\rm in}, \\
b_t &= -i\sqrt{k_2}a.
\end{aligned} \tag{A11}$$

Thus we get the Heisenberg-Langevin equations (2).

[1] Q. A. Turchette, C. J. Hood, W. Lange, H. Mabuchi, and H. J. Kimble, Phys. Rev. Lett. **75**, 4710 (1995).

[2] L. M. Duan and H. J. Kimble, Phys. Rev. Lett. **92**, 127902 (2004).

[3] J. Cho and H.-W. Lee, Phys. Rev. Lett. **95**, 160501 (2005).

[4] H. Oka, S. Takeuchi, and K. Sasaki, Phys. Rev. A **72**, 013816 (2005).

[5] F. H. Holger, K. Kunihiro, T. Shigeki, and S. Keiji, J. Opt. B: Quantum Semiclassical Opt. **5**, 218 (2003).

[6] A. Auffèves-Garnier, C. Simon, J.-M. Gérard, and J.-P. Poizat, Phys. Rev. A **75**, 053823 (2007).

[7] T. G. Tiecke, J. D. Thompson, N. P. de Leon, L. R. Liu, V. Vuletic, and M. D. Lukin, Nature (London) **508**, 241 (2014).

[8] D. Englund, A. Faraon, I. Fushman, N. Stoltz, P. Petroff, and J. Vuckovic, Nature (London) **450**, 857 (2007).

[9] H. F. Hofmann and H. Nishitani, Phys. Rev. A **80**, 013822 (2009).

[10] L. M. Duan, A. Kuzmich, and H. J. Kimble, Phys. Rev. A **67**, 032305 (2003).
[11] K. Zhang and Z.-Y. Li, Phys. Rev. A **81**, 033843 (2010).
[12] C. Wang, J. Mod. Opt. **59**, 962 (2012).
[13] T. Volz, A. Reinhard, M. Winger, A. Badolato, K. J. Hennessy, E. L. Hu, and A. Imamoglu, Nature Photon. **6**, 605 (2012).
[14] W. Chen, K. M. Beck, R. Buecker, M. Gullans, M. D. Lukin, H. Tanji-Suzuki, and V. Vuletic, Science **341**, 768 (2013).
[15] J. Volz and A. Rauschenbeutel, Science **341**, 725 (2013).
[16] A. Reiserer, S. Ritter, and G. Rempe, Science **342**, 1349 (2013).
[17] A. Szoke, V. Daneu, J. Goldhar, and N. Kurnit, Appl. Phys. Lett. **15**, 376 (1969).
[18] A. Baas, J. P. Karr, H. Eleuch, and E. Giacobino, Phys. Rev. A **69**, 023809 (2004).
[19] T. Elsässer, B. Nagorny, and A. Hemmerich, Phys. Rev. A **69**, 033403 (2004).
[20] Y. Dumeige, A. M. Yacomotti, P. Grinberg, K. Bencheikh, E. Le Cren, and J. A. Levenson, Phys. Rev. A **85**, 063824 (2012).
[21] S. Yang, M. Al-Amri, and M. S. Zubairy, Phys. Rev. A **87**, 033836 (2013).
[22] A. T. Rosenberger, L. A. Orozco, H. J. Kimble, and P. D. Drummond, Phys. Rev. A **43**, 6284 (1991).
[23] C. F. Marki, D. R. Jorgesen, H. Zhang, P. Wen, and S. C. Esener, Opt. Express **15**, 4953 (2007).
[24] M. J. Adams, Solid-State Electron. **30**, 43 (1987).
[25] C. Savage and H. Carmichael, IEEE J. Quantum Electron. **24**, 1495 (1988).
[26] N. Mitchell, J. Connolly, J. O'Gorman, and J. Hegarty, Opt. Lett. **19**, 269 (1994).
[27] Y. Li, L. Aolita, D. E. Chang, and L. C. Kwek, Phys. Rev. Lett. **109**, 160504 (2012).
[28] C. W. Gardiner and M. J. Collett, Phys. Rev. A **31**, 3761 (1985).
[29] D. F. Walls and G. J. Milburn, *Quantum Optics* (Springer, New York, 2007).
[30] A. V. Malyshev, Phys. Rev. A **86**, 065804 (2012).
[31] X. Xia, J. Xu, and Y. Yang, J. Opt. Soc. Am. B **31**, 2175 (2014).
[32] L. M. Duan, Nature (London) **508**, 195 (2014).
[33] E. Yüce, G. Ctistis, J. Claudon, E. Dupuy, R. D. Buijs, B. de Ronde, A. P. Mosk, J.-M. Gérard, and W. L. Vos, Opt. Lett. **38**, 374 (2013).